J. Fluid Mech. (2000), *vol.* 415, *pp.* 175–202. Printed in the United Kingdom

Surface pressure fluctuations on aircraft flaps and their correlation with far-field noise

By Y. P. GUO, M. C. JOSHI, P. H. BENT AND K. J. YAMAMOTO

The Boeing Company, Mail Code C078-0420, 2401 E. Wardlow Road, Long Beach, CA 90807, USA

(Received 4 June 1999 and in revised form 6 March 2000)

This paper discusses unsteady surface pressures on aircraft flaps and their correlation with far-field noise. Analyses are made of data from a 4.7% DC-10 aircraft model test, conducted in the 40×80 feet wind tunnel at NASA Ames Research Center. Results for various slat/wing/flap configurations and various flow conditions are discussed in detail to reveal major trends in surface pressure fluctuations. Spectral analysis, including cross-correlation/coherence, both among unsteady surface pressures and between far-field noise and near-field fluctuations, is used to reveal the most coherent motions in the near field and identify potential sources of noise related to flap flows. Dependencies of surface pressure fluctuations on mean flow Mach numbers, flap settings and slat angles are discussed. Dominant flow features in flap side edge regions, such as the formation of double-vortex structures, are shown to manifest themselves in the unsteady surface pressures as a series of spectral humps. The spectral humps are shown to correlate well with the radiated noise, indicating the existence of major noise sources in flap side edge regions. Strouhal number scaling is used to collapse the data with satisfactory results. The effects of flap side edge fences on surface pressures are also discussed. It is shown that the application of fences effectively increases the thickness of the flaps so that the double-vortex structures have more time to evolve. As a result, the characteristic timescale of the unsteady sources increases, which in turn leads to a decrease in the dominant frequency of the source process. Based on this, an explanation is proposed for the noise reduction mechanism of flap side edge fences.

1. Introduction

Surface pressure fluctuations can be used to understand the physics of the flow features that produce the fluctuations, wall pressure spectra under turbulent boundary-layer flows being a typical example (e.g. Blake 1986). In these cases, the surface pressure fluctuations are regarded as the footprints of the flow, and much useful information can be extracted from them. In acoustic applications, it is known that unsteady surface pressures are one of the dominant controlling parameters for the far-field radiation, which can lead to direct predictions of the radiated noise (Curle 1955; Ffowcs Williams & Hawkings 1969; Howe 1978; Brooks & Hodgson 1981). Furthermore, when measured together with far-field noise, surface pressure fluctuations can be used to identify potential noise sources through the technique of near-field/far-field cross-correlation/coherence analysis (e.g. Ahtye, Miller & Meecham 1979; McInerny, Meecham & Soderman 1990). This provides a potentially very powerful tool for noise

source identification and characterization in environments with poor signal to noise ratio, as is the case for airframe noise tests in wind tunnels. In this paper, we will discuss the features of unsteady surface pressures on aircraft flaps and their correlation with far-field radiation. Analysis will be made of the data from a 4.7% DC-10 aircraft model test conducted in the 40×80 feet wind tunnel at NASA Ames Research Center. The test facility and measurement implementation will be described in § 2. In addition to surface pressures, measurements are also made for far-field noise, including noise spectra and directivities by free field microphones and source amplitudes by a phased microphone array. The far-field results and analyses will, however, be given elsewhere (Guo *et al.* 1998), while the unsteady surface pressures will be the main focus here.

The surface pressure data are acquired and analysed for various high-lift system configurations and under various flow conditions. In general, the deployment of any component of the high-lift system, namely, flaps and slats, increases the levels of the surface pressure fluctuations and the higher the deployment angles, the higher the surface pressure fluctuations. This explains the general trends observed in the far-field data that the higher the deployment angles for the high-lift system components, the higher the noise levels (Guo *et al.* 1998), because the noise radiation can be attributed to the surface pressures (Curle 1955; Ffowcs Williams & Hawkings 1969). The variations of the surface pressures with the flap/slat settings are found to be relatively uniform in frequency. For example, when the flap deployment angle doubles from 25° to 50°, the surface pressure spectra are found to increase by more than 10 dB almost uniformly in the entire frequency domain.

Because of the high Reynolds numbers associated with flows in the vicinity of aircraft high-lift systems, the flows over the flaps and slats are mostly fully developed turbulent flows. This will be demonstrated by the scaling of the surface pressure spectra; the normalized spectra show features, such as the high-frequency fall-off, very similar to those observed in turbulent boundary-layer flows. The well-developed turbulent flows are found on the main surfaces of the flaps where the surfaces have large radii of curvature, and, hence, essentially behave like flat plates. They are also observed in regions close to the side edges of the flaps near the thrust gate, where the local non-uniform features due to the edges are overwhelmed by the high turbulence levels of the incoming flows. The high levels of turbulence may result from the nacelle and/or the landing gear, both being upstream of the thrust gate.

An important exception of this turbulent-flow behavior is the outboard edge of the outboard flap, where the incoming flow is relatively clean and the flow is dominated by local features, namely, the highly coherent double-vortex structures. These vortex structures may result from flow separation at the corners of the flap side edge, owing to the inability of the cross-flow to follow the abruptly changing surface contours of the flaps (e.g. Guo 1999). They manifest themselves in the surface pressure fluctuations in terms of a series of spectral humps. These humps have also been observed in the past for simplified flaps and wing tips (McInerny *et al.* 1990; Horne *et al.* 1997). By studying the spatial variations of the surface pressure spectra in the flap side edge regions, we will show that the humps follow the evolution of the double-vortex structures; they are most clearly seen by surface pressure sensors in the helical roll-up path of the vortex structures. The spectral humps are the most coherent features in the surface pressures. They have cross-coherence coefficients as high as 0.8 and cover a bandwidth of up to 4 kHz. It will be shown that these spectral humps are also well correlated to the far-field noise. A comparision of far-field/near-field correlation at various spanwise locations will show the highest correlation at the outboard edge of the outboard flap, indicating the existence of major noise sources in this region.

The peak frequencies of the spectral humps will be shown to scale on the Strouhal number based on the free-stream velocity and a lengthscale. The latter characterizes the coherence length of the vortical patches, and, hence, is Reynolds-number dependent. By using this scaling, the humps can be collapsed to a Strouhal number of about 0.9 and its integer multiples, which are the frequencies of the harmonics of the primary hump, resulting from the fully nonlinear nature of the flows. The concept of using a Reynolds-number-dependent lengthscale is, in fact, routinely used in studies on wall pressures under turbulent boundary-layer flows (e.g. Blake 1986), in which case, the momentum thickness of the turbulent boundary layer is one of the choices. For the flap side edge flow, the coherence structures have been studied and understood much less than the turbulent boundary-layer flow, so there are no existing guidelines to follow. To proceed with our data analysis, we will derive an order of magnitude estimate for the lengthscales, which will be shown to yield satisfactory results.

The effects of flap side edge fences on the surface pressures will also be discussed because side edge fences have been studied in recent years as a potential noise reduction device (Ross, Storms & Kumagai 1995; Storms *et al.* 1996; Guo *et al.* 1998). Whereas a reduction of a few dB in flap-related noise has been observed, there has not been a conclusive understanding of the physical mechanisms by which the noise is reduced. It is likely that the noise reduction is due to the joint effects of more than one mechanism, including the change of source spectral characteristics. We will present data to support this particular mechanism, in the form of the downward shift of the hump peak frequencies when fences are applied. An explanation of this may be the effective increase of the flap thickness owing to the fences. The evolution of the double-vortex structure is essentially characterized by the timescale of the vortex motions in the thickness direction because of the vortex–edge interaction. With increased thickness, the vortex structures have more time to evolve before they have to interact with the sharp corners. Correspondingly, the longer characteristic time when fences are applied leads to lower characteristic frequency for these cases, and, hence, a downward shift of the source spectra. This in turn causes a downward shift of the far-field noise spectra. Even without any reduction in source strength, this downward shift in frequency may appear as a noise reduction. This is because airframe noise typically has a spectrum with a negative slope in almost the entire mid- to high-frequency domain, which is also the most sensitive domain for aircraft noise certification. Thus, for any fixed frequency bands, a downward shift of the spectrum replaces the noise levels in these bands with the lower levels at higher frequencies. In this way, a reduction in noise level is achieved for fixed frequency bands even if the total radiated acoustic energy remains unchanged. It is appropriate to point out that our limited database does not enable us to show conclusively whether there is a weakening in source strength owing to the fences, which may also contribute to the observed reduction in far-field noise. The surface-pressure data, however, does reveal the downward shift in the characteristic frequencies of the flow features. Thus, it is likely that at least some part of the noise reduction due to flap side edge fences comes from the shift of the acoustic energy out of the frequency bands that are important to aircraft noise certification.

2. Test facility, measurement implementation and data analysis

The analyses presented in this paper are based on data from a test using a 4.7% small-scale model of the McDonnell DC-10-30 transport airplane. Its high-lift system consists of two partial-span, single-element slats and two partial-span, single-element

flaps, which are respectively, called the inboard and the outboard slat/flap. The engines on the model aircraft are modelled as flow-through devices without power. Both the slats and the flaps on the small model are adjustable. The model has a wingspan of approximately 8 feet, and it is a true scale-down of the DC-10 configuration; the small-scale model has all the components, including all the stabilizers and landing gears. The test facility is the 40×80 feet wind tunnel at NASA Ames Research Center, which is a closed-flow facility with partial acoustic treatment. The model is mounted with a sting connected with a knife-blade-type support. The height of the model in the facility was determined by reproducing the FAA fly-over altitude of 394 feet (120 m) at model scale. A sting mount was chosen to provide as great a distance as possible between the support system and the model, in order to reduce the potential contamination of the radiated noise measurements by noise generated on the support.

For measuring unsteady surface pressures, there are 29 sensors (23 Endevco and 6 Kulite) implemented on one wing of the model. They are flush-mounted on the surface of the high-lift system at various locations, mostly on the flaps. There are only two sensors on the leading-edge slat and both are located on the upper surface. The sensors on the two flaps can be conveniently divided into four major groups according to their geometrical locations. They are the mid-span of the inboard flap, the outboard edge of the inboard flap, the inboard edge of the outboard flap and the outboard edge of the outboard flap. The locations of these groups are all shown in figure 1, together with two trailing edge sensors. The sensors on the side surfaces of the flaps are approximately located on the centerline of the flap cross-section. Those on the upper and lower surfaces are positioned quarter of an inch away from the edges except for those at the inboard edge of the outboard flap where the small flap thickness makes it very difficult to implement the sensors close to the flap side surface. As a result, the sensors at this edge are located half an inch away from the side edge. The locations and labelling of the sensors are also summarized in table 1. The numbers in the column for the chordwise locations are the percentage of the local chord, from the flap leading edge. More detailed sensor locations and labelling for the outboard edge of the outboard flap are given in figure 2 for the convenience of later discussions, a large part of which will be related to this location.

The signals of the unsteady pressure sensors are acquired through three Metron recorders, respectively labelled A, B and M, and each having 16 channels. Because of the limitation of the number of available channels on each Metron recorder, the sensors are divided into three groups. Each group has 12 channels for unsteady surface pressures, and the remaining 4 channels in each Metron recorder are assigned to four far-field noise signal measurements so that far-field/near-field correlation analysis can be performed. Of the four far-field noise measurements, two are from the pole-mounted free field microphones, located 4.25 feet under the wing, and the other two are from two microphones in the phased microphone array (see Guo *et al.* 1998 for detailed acoustic measurement implementation). Signals within each group are synchronized for cross-coherence/correlation analysis but no attempt is made to synchronize signals in different groups. However, two sensors in each group are selected to be simultaneously recorded in other groups to monitor the cross-correlation between the geometrically separated groups, as can be seen also in table 1 in the column for Metron channels. Our analysis shows that there is little coherence between sensors in different groups, because these groups are located quite far away from each other. The separations, both streamwise and spanwise, between the groups are much larger than the coherence lengths of the unsteady motions in the flow so that the flow field at each location can be analysed independently.

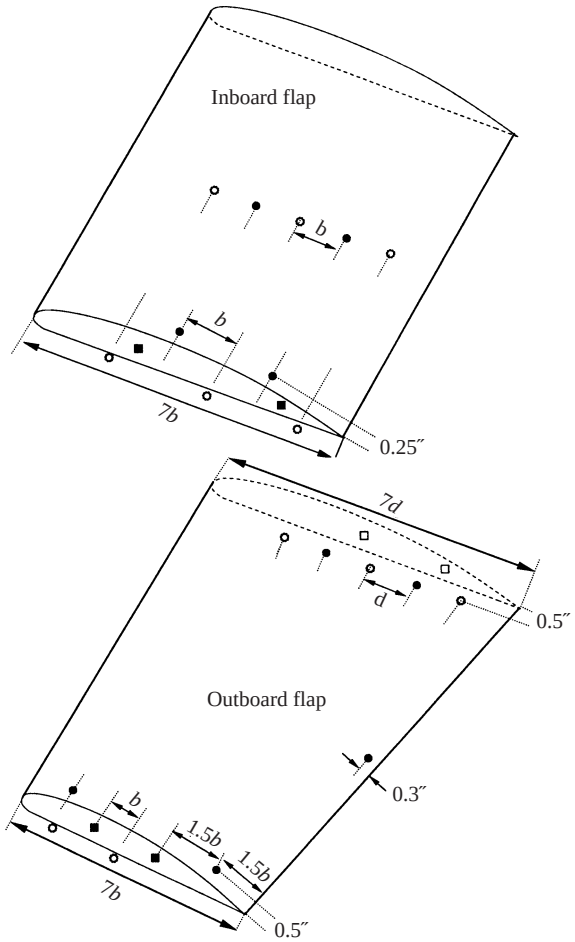

FIGURE 1. Locations of unsteady surface pressure sensors on the two flaps: ●, upper surface; ○, lower surface; ■, side surface.

The tests were carried out for various aircraft configurations and flow conditions. There were 33 runs in which unsteady surface pressures were measured. The flow conditions in the tests are mainly controlled by the free-stream flow Mach number M, with three values

$$M = 0.2, \quad 0.25, \quad 0.275.$$

The high-lift systems are controlled by the flap angle δ_F with four settings

$$\delta_F = 0^\circ, \quad 25^\circ, \quad 35^\circ, \quad 50^\circ,$$

and the slat angle δ_S, either retracted or deployed,

$$\delta_S = 0^\circ, \quad 20^\circ,$$

where zero degree means the component is retracted. Landing gears are also modelled on the small-scale aircraft and are tested both on and off. The size of the model gears, however, does not allow a true scale-down of the real landing gears and the variations due to the deployment or the small gears may not be reliable so that no results will be presented here.

Sensor	Spanwise location	Surface	Chordwise location	Metron channel
SP1			28,6	A5
SP2	Mid span	Lower surface	57,1	A6
SP3	Inboard flap		85,7	A7
SP4		Upper surface	42,9	A8,M11
SP5			71,4	A9,M12
SP6			28,6	A10
SP7		Lower surface	57,1	A11
SP8	Outboard edge		85,7	A12
SP9	Inboard flap	Upper surface	42,9	A13,M13
SP10			71,4	A14,M14
SP24		Side surface	35,7	A15
SP25			78,6	A16
SP11			28,6	B5
SP12		Lower surface	57,1	B6
SP13	Inboard edge		85,7	B7
SP14	Outboard flap	Upper surface	42,9	B8
SP15			71,4	B9
SP26		Side surface	35,7	B10
SP27			78,6	B11
SP16	Mid span	Lower surface	0.3 in. from TE	B12
SP17	Outboard flap	Upper surface	0.3 in. from TE	B13
SP18		Lower surface	14,3	M5
SP19			42,9	M6
SP20	Outboard edge	Upper surface	14,3	M7
SP21	Outboard flap		78,6	M8
SP28		Side surface	28,6	M9
SP29			57,1	M10
SP22	Inboard slat	Upper surface	LE	M15,B14
SP23			LE	M16,B15

TABLE 1. Locations and grouping of the unsteady surface pressure sensors. The numbers in the 'Chord-wise location' column are the percentage of local flap chord from its leading edge.

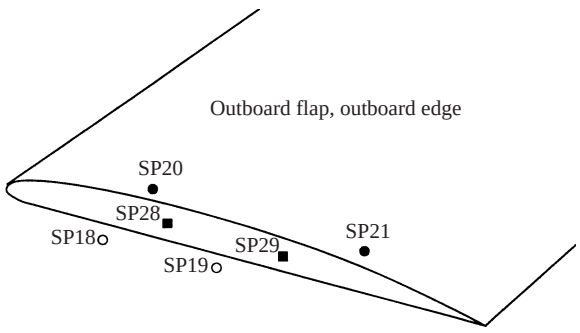

FIGURE 2. Sensor locations and labelling at the outboard edge of the outboard flap: ●, upper surface; ○, lower surface; ■, side surface.

Flap side edge fences are also tested. They are extension plates vertically attached to the side edges of the flap. They are contoured exactly the same on the top side as the upper surface of the flap so that their top sides are flash mounted with the upper surfaces of the flaps. The lower sides of the fences extend beyond the lower surface

contours of the flaps so that the cross-flow is somehow blocked by the fences. The fences are characterized by their height h, which is defined by the part extending into the flow. Three values of h are tested, namely,

$$h = 0.5\,t_F, \quad 1.0\,t_F, \quad 2.0\,t_F,$$

where t_F is the maximum flap thickness at the side edges. Some other changes are also made in the tests, such as sealing the hinges and fairing the flaps, but no significant effects are found in the data owing to these configuration variations. Boundary-layer tripping is also tested on various components to ensure fully developed turbulent boundary-layer flow. Again, comparisons with non-tripped cases do not reveal any noticeable effects.

All the signals, both unsteady surface pressures and sound pressure fluctuations, are recorded simultaneously as time series data at a sampling rate of 80 kHz with usable frequencies of up to 20 kHz. The coherence and correlation analysis is carried out by using standard spectral analysis which performs fast Fourier transform (FFT) on the time series data, takes ensemble averages and calculates spectral quantities, including power spectra and cross-coherence coefficients. Correlation coefficients are then computed from the complex coherence coefficients by inverse FFT. To ensure data stationarity, each FFT uses 2048 data points with no overlap, which corresponds to 25.6 ms of data at a sampling rate of 80 kHz, which is sufficient because it takes less than 4 ms for sound waves orginating from the model to reach the microphones. Studies have also been carried out to check the stationarity of the data by taking different time segments of data and comparing their spectral properties, which show very good consistency. Convergence studies have been carried out before the data reduction, which show that good convergence can usually be achieved with about 300 to 400 averages for cross-coherence (autocoherence requiring much less). The automated data reduction process actually takes 600 averages, which gives a sufficient safety margin to ensure convergence.

3. Effects of side edge flow separation

A most prominent feature in flap side edge flows is the formation of double-vortex structures. This has been observed in the past and has recently been studied in great detail both numerically and experimentally (Mathias *et al.* 1995; Meadows *et al.* 1997; Khorrami, Singer & Radeztsky 1998; Radeztsky, Singer & Khorrami 1998). These double-vortex structures result from the inevitable flow separation of the spanwise cross-flow, and their inherently unsteady nature is believed to be a major source of unsteadiness in the flow. The unsteady fluctuations are evident in the surface pressures in the form of very distinct multiple spectral humps, as observed in simple wing/flap geometry experiments (McInerny *et al.* 1990). The amplitudes and the peak frequencies of these humps vary with high-lift system configurations and flow conditions, but they almost always appear in the spectra as long as the flaps are deployed. Some examples of these are shown in figure 3, which plots the surface pressure spectrum in dB, defined by

$$10 \log \frac{E(f)\Delta f}{(20\,\mu\text{Pa})^2}, \tag{3.1}$$

where E is the pressure spectra, a function of frequency f, and Δf is the frequency band equal to 64 Hz. The case shown in this figure is for flow Mach number $M = 0.275$, flaps and slats respectively deployed at 50° and 20° and landing gears retracted. The

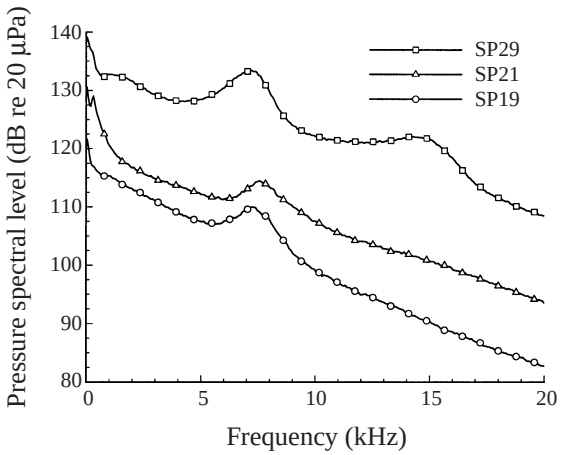

FIGURE 3. Surface pressure spectra in the aft half-chord region at the outboard edge of the outbaord flap for the case of $M = 0.275$, flaps and slats deployed, respectively, at 50° and 20° and landing gears retracted.

three sensors are located in the aft half-chord region at the outboard edge of the outboard flap, as shown in figure 2. Evidently, the spectra are dominated by the humps at about 7.5 kHz and its integer multiples. This figure is, in fact, representative of all data for other test conditions, although the levels and frequencies of the humps may vary, as will be discussed later.

It is interesting to note that the three sensors that see the spectral humps are all located in the helical path of the double-vortex structure. For comparison, the spectra at the three sensors in the forward half-chord region at the same side edge are plotted in figure 4, showing essentially a gradual fall-off shape and the absence of the humps. This indicates that these spectral humps are associated with the unsteady motions of the vortex structures. From recent steady CFD computation and near field-flow measurements (Mathias *et al.* 1995; Meadows *et al.* 1997; Khorrami *et al.* 1998; Radeztsky *et al.* 1998), it is known that flow separation usually occurs near the lower corner of the flap side surface. Because of the cross-flow due to the static pressure difference between the upper and the lower surface of the flap, the highly vortical separated flow is rolled up around the flap side face along a helical path. As it moves along this helical path, it grows both in size and intensity to form a well-defined vortex. Because of the highly unsteady nature of the flow-separation process, the flap side edge vortex may experience various kinds of unsteady motions such as spinning, stretching and oscillation around its equilibrium position. Though these unsteady motions may not all cause acoustic radiation, they all manifest themselves in the surface pressures, especially in the aft half-chord region because the helical vortex essentially covers this part of the flap. This is exactly what is shown in figures 3 and 4 where the sensors in the aft half-chord region all recorded distinctive humps at about 7.5 kHz and its integer multiples. Those in the forward half-chord region away from the helical roll-up path do not show this feature because the aerodynamic fluctuations decay exponentially away from the sources.

These spectral humps, in fact, represent the most coherent motions in the flow near the flap side edges. To demonstrate this, the coherence coefficients between the three sensors in the aft half flap-chord region, namely, SP19, SP29 and SP21, are plotted in figure 5 for the same test conditions as those in figure 3. Evidently,

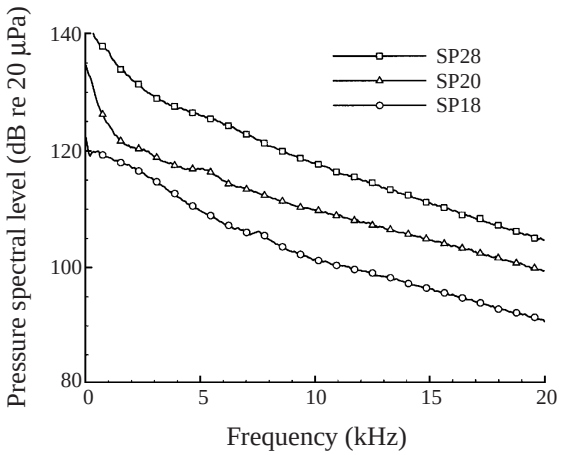

FIGURE 4. Surface pressure spectra in the forward half-chord region at the outboard edge of the outboard flap for the case of $M = 0.275$, flaps and slats deployed, respectively, at 50° and 20° and landing gears retracted.

the unsteady motions at about 7.5 kHz are highly coherent; the amplitudes of the coherence coefficient exceed 0.8. The high coherence is centred at about 7.5 kHz and covers a broad frequency band from about 6 kHz to 9 kHz. Because the flow is highly nonlinear, strong coherence can also be seen at harmonics of the primary hump, for example, at about 15 kHz, even though the surface pressure spectra plotted in figure 3 do not always show very distinctive humps at these harmonics.

High coherence levels exceeding 0.8 can also be seen in the low-frequency parts in figure 5. As will be seen later in the paper, there is almost always high coherence at low frequencies for sensors within each of the four groups and for all the flow conditions and high-lift system configurations. This results from the coherent turbulent boundary-layer flows. At low frequencies, the typical lengthscale for the coherent turbulent boundary-layer flows is larger than the physical separations between the sensors within a group so that pressure fluctuations recorded by the sensors are highly coherent.

The locations of the unsteady sources that cause the spectral humps in relation to the sensor locations can be identified by cross-correlation analysis of the surface pressures. Shown in figure 6 are the cross-correlation coefficients between SP19, SP29 and SP21 for the same test conditions as those in figures 3 and 5. The frequency band for the correlation calculations is from 5 kHz to 10 kHz, which is the band covered by the humps in the pressure spectra. The reference sensor in this figure is SP29, located on the side surface approximately on the centreline of the flap thickness (see figure 2). Thus, the diagram in the middle of figure 6 is actually the autocorrelation, as shown by the symmetrical shape of the curve and the unity amplitude at zero time delay. The top diagram is the correlation between SP21, located on the upper surface of the flap, and the side surface sensor SP29. It shows that the peak correlation appears at approximate zero time delay, suggesting that the source of the unsteady motions must be located at approximately equal distance from both SP29 and SP21. This is in the region close to the upper corner of the flap side surface. This conclusion can also be derived from the bottom diagram of figure 6, which shows the correlation between the lower surface sensor SP19 and the side surface sensor SP29. It can be seen in this diagram that the peak correlation has a negative time delay, meaning that the

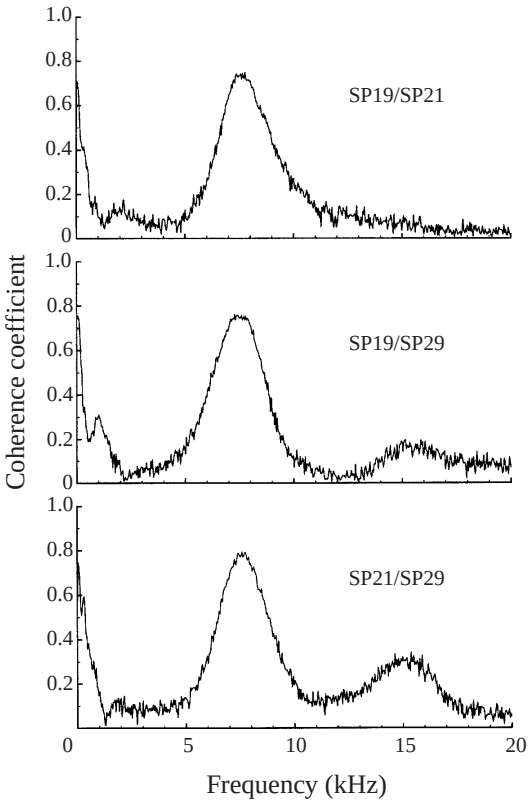

FIGURE 5. Cross-coherence between sensors in the aft half-chord region at the outboard edge of the outboard flap for the case of $M = 0.275$, flaps and slats deployed, respectively, at 50° and 20° and landing gears retracted.

side surface sensor SP29 receives the unsteady disturbances before the lower surface sensor SP19 does. This again suggests that the location of the unsteady source is somewhere near the upper corner of the flap side face.

The above analysis shows that the vortex structure close to the upper corner of the flap side surface is probably the dominant unsteady source that causes the spectral hump at about 7.5 kHz. It does not, however, provide any explanation as to why this is so. The unsteady surface pressure data alone is clearly not sufficient to achieve an understanding of this issue. Here, we suggest a possible reason, based on the limited evidence from the data and obviously needing future confirmation. It can be argued that a vortex structure produces unsteady fluctuation most efficiently when it interacts with a sharp edge or corner. In this view, the magnitude of flow unsteadiness is controlled by how strong the vortex/edge interaction is, which is in turn determined by the combined effects of the strength of the vortex and its closeness to the edge. The stronger the vortex and/or the closer it is located to the edge, the stronger the interaction, and hence, the larger the magnitude of the unsteady motions. In the region close to the lower corner of the flap side surface, the vortex may be very close to the sharp corner, but it has relatively small strength because it has just been formed and has not had enough time to evolve. The vortex/edge interaction in this region is thus relatively weak. The interaction is also weak for a vortex above the upper surface of the flap because the vortex in this region has been convected away

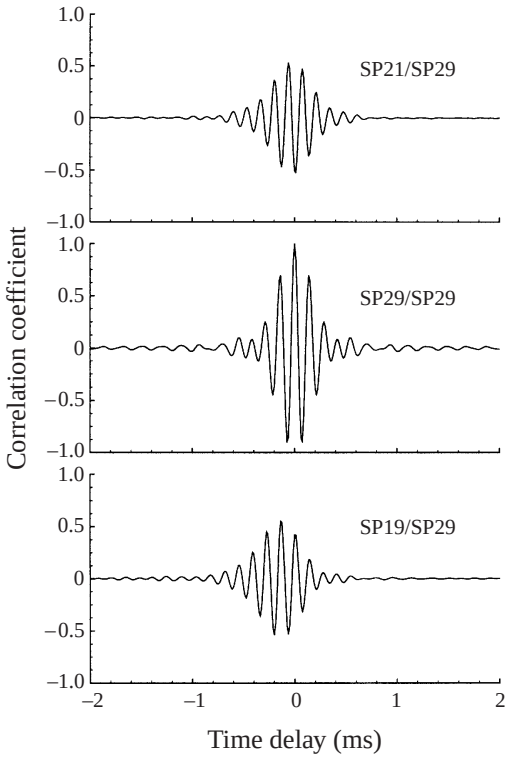

FIGURE 6. Correlation coefficients for sensors in the aft half-chord region at the outboard edge of the outboard flap for the case of $M = 0.275$, flaps and slats deployed, respectively, at 50° and 20° and landing gears retracted.

from the corners, even though the vortex size and strength has grown to significant levels. In between these two cases at the locations close to the upper corner of the side edge, the vortex has grown significantly along the helical path covering the entire flap cross-section, and as it rolls up, it can become very close to the upper corner of the side surface. The combined effects of vortex strength and location relative to a sharp corner then make the vortex close to the upper corner of the flap side surface a very efficient source of unsteady motions.

4. Strouhal number scaling

It is clearly of interest to examine the scaling of the spectral humps in the surface pressures in order to identify possible trends in the unsteady motions, which may be used in future modelling and/or experimental studies. For flap side edge flows, however, there are few guidelines that we can follow to scale the data. There has been very little systematic research in the past on flows in complex conditions such as those in aircraft flap side edge regions, which involve complicated static pressure loading, flow separations and aerodynamic interactions between components in the high-lift system. The scaling analysis is made even more difficult by the scarcity of the flow information such as boundary-layer properties and local flow velocity. These are not considered in our tests either, because they are not the original objectives of these particular tests. Nevertheless, some efforts will be made here to scale the data with some hypotheses and assumptions. It is then appropriate to point out that the results

given in the following should be checked and confirmed by future tests to validate the hypotheses.

An important parameter in scaling the surface pressures is the characteristic length of the unsteady motions. A first intuitive choice may be the thickness of the flap, or other fixed length associated with the aircraft model, as is conventionally assumed in extrapolating small-scale test data to large-scale applications (e.g. Allen & Soderman 1997; Hayes *et al.* 1997). This, however, may not always be the most proper choice because it is independent of flow conditions. It is reasonable to argue that the dominant lengthscale of the flow process that produces unsteady motions is very likely to be a function of the flow conditions and there are many examples to illustrate this. For instance, pressure fluctuations under turbulent boundary layers on flat surfaces scale better on the momentum thickness of the boundary-layer flow, rather than any physical dimensions of the surfaces on which the boundary layers are formed. The momentum thickness itself is, of course, a function of the local flow Reynolds number (e.g. Blake 1986). In the present case of flap side edge flow, the characteristic lengthscale is likely to be the coherence length of the vortex structure, which itself is likely to vary with flow conditions and flap geometry. At present, information on this quantity is not yet available so that we will assume that it is of the same order as the local momentum thickness of the turbulent boundary layer at the trailing edge of the flap.

To derive a reasonable order of magnitude estimate for the characteristic lengthscale, we argue that, similarly to boundary layers of zero pressure gradient, the boundary-layer thickness varies with the local Reynolds number to a certain power and is proportional to the local distance from the separation point. This leads to the expression

$$\delta^* = \beta x R_x^{\mu}, \tag{4.1}$$

where δ^* denotes the local boundary-layer momentum thickness, β and μ are numerical constants and R_x is the Reynolds number based on x, the local distance from the separation point, approximately equal to the distance from the leading edge of the flap, which is given by the conventional definition

$$R_x = xU_0/v, \tag{4.2}$$

with U_0 being the free-stream velocity and v the kinematics viscosity. If this kind of dimensional argument holds, the constants β and μ in (4.1) should be true numerical constants independent of flow parameters and should be determined by experimental data. To do so, we use the results from Brooks & Hodgson (1981) for turbulent boundary layers on isolated airfoils. They measured the momentum thickness at the trailing edges of airfoils and fitted the data to an expression

$$\delta^* = 0.0601 \times 10^{g}\, cR_c^{-0.114}, \tag{4.3}$$

for R_c less than about 0.3×10^6, where R_c is the Reynolds number based on the airfoil chord c. In this data fitted result, g is a function of the angle of attack of the airfoil, which is also derived by fitting experimental data,

$$g = -0.0432\alpha + 0.00113\alpha^2, \tag{4.4}$$

with α denoting the angle of attack of the airfoil.

The Reynolds number based on the flap chord in our tests is approximately within this range, so that if our hypothesis (4.1) is reasonable and the data fitted result (4.3) is applicable, equations (4.1) and (4.3) should be equal when x in (4.1) is replaced by

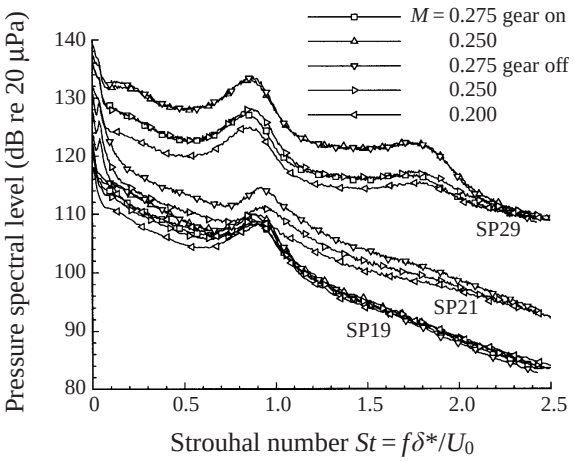

FIGURE 7. Normalized surface pressure spectra for various test conditions for sensors in the aft half-chord region at the outboard edge of the outboard flap with slats deployed at 20°.

the flap chord c. This determines the exponential factor of the Reynolds number to be -0.114, since the Reynolds number is the only parameter that involves the flow velocity. This process also determines the numerical constant β in (4.1) as

$$\beta = 0.0601 \times 10^{g}. \tag{4.5}$$

With the choice of δ^* as the reference lengthscale and by choosing the free-stream velocity U_0 as the velocity scale, the frequency f can be normalized by the Strouhal number,

$$St = f\delta^*/U_0. \tag{4.6}$$

This frequency scaling turns out to be quite satisfactory for the spectral humps in the surface pressures in our tests. Figures 7 and 8 show some results at different flow conditions. It is clear that the spectral humps are all scaled to a Strouhal number of about 0.9, both for different test conditions and for different sensor locations. It can be seen that there is no amplitude normalization for the pressure spectra in these two figures and the level of the spectral humps varies quite significantly from sensor to sensor. Amplitude scaling is not attempted for the spectral humps because the unsteady flow at this peak frequency is dominated by the well-defined roll-up vortex and hence is highly non-homogeneous. Because the amplitude of the aerodynamic pressures decays exponentially away from the unsteady sources, the amplitude of the spectral humps is very sensitive to the locations of the sensor with respect to the locations of the helical vortex patch, which itself varies with flow conditions and flap geometry. The unsteady pressure sensors in our tests are quite sparsely located in reference to the characteristic length of the coherent aerodynamic field so that it is unlikely that consistent trends can be extracted from this incomplete database.

The above analysis shows that the spectral humps collapse at the same Strouhal number for different flow conditions. This can be used to derive the dependence of the peak frequencies of the surface pressure spectra on flow parameters such as the free-stream velocity. By setting the Strouhal number to constant and by using the definition of the momentum thickness (4.1), it can be found that

$$f_{\text{peak}} \propto U_0^{\gamma} \quad \text{with} \quad 1.1 \leqslant \gamma \leqslant 1.2. \tag{4.7}$$

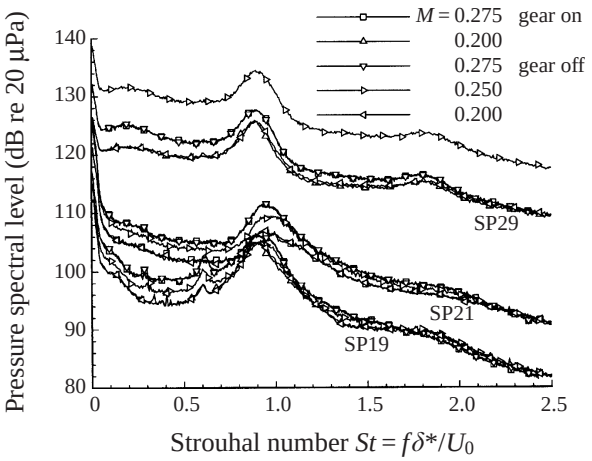

FIGURE 8. Normalized surface pressure spectra for various test conditions for sensors in the aft half-chord region at the outboard edge of the outboard flap with slats retracted.

The scaling by the reference lengthscale (4.1) actually leads to $\gamma = 1.114$ if the data fitted result (4.3) is used. To account for possible variations due to the uncertainty involved in the scaling and data fitting, we take this particular value of γ as a mean value and extend its range as indicated in the above result. The upper bound $\gamma = 1.2$ corresponds to the case of a fully developed turbulent boundary layer.

An important implication of the analysis given above on Strouhal-number scaling is the Reynolds-number effect on frequency scaling when extrapolating small-scale model experimental data to full-scale tests, which is an important but not yet resolved issue. The conventional way of extrapolating frequency from small- to full-scale is simply a multiplication of the physical scale factor, namely, the ratio of the physical dimensions of the models (e.g. Allen & Soderman 1997; Hayes *et al.* 1997). This is the correct scaling if the characteristic length of the unsteady process is independent of the flow conditions. In the present case, the lengthscale is very likely to be flow-dependent, as analysed in the previous paragraphs and given by (4.1) or (4.3) as a function of the Reynolds number. Thus, the frequency extrapolation must follow a different scaling law. This scaling law can be derived by equating the Strouhal number in the small-scale model experiments to that in the full-scale application. In experimental studies, the flow Mach number can usually be maintained the same for both cases. In this event, the definition of the Strouhal number (4.6) immediately leads to

$$f_{\text{full}}\,\delta^*_{\text{full}} = f_{\text{small}}\,\delta^*_{\text{small}}, \tag{4.8}$$

where the subscripts 'full' and 'small', respectively, indicate quantities in full-scale and small-scale tests. By further using the definition of the characteristic lengthscale such as (4.1), the frequency ratio can be found to be

$$\frac{f_{\text{full}}}{f_{\text{small}}} = \frac{\delta^*_{\text{small}}}{\delta^*_{\text{full}}} = \frac{L_{\text{small}}}{L_{\text{full}}}\left(\frac{R_{\text{small}}}{R_{\text{full}}}\right)^{\mu} = \left(\frac{L_{\text{small}}}{L_{\text{full}}}\right)^{2-\gamma}, \tag{4.9}$$

where the last step comes from using the definition of the Reynolds number (4.2) with x replaced by L, the physical dimension of the model, and the value of γ is given by (4.7). This shows that the frequencies of full-scale tests and small-scale model experiments are related by the physical scale factor of the models to a power

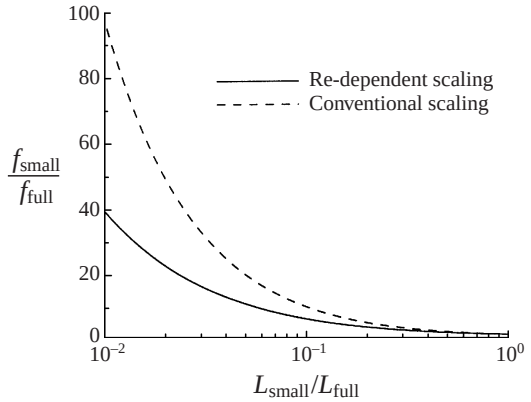

FIGURE 9. Comparison of different frequency scaling laws.

that is less than one, in contrast to the linear dependence that is usually used and is independent of the Reynolds number. This Reynolds-number-related scaling is especially important when very small models are used to simulate full-scale models. In our DC-10 small-scale-model tests, for example, the scale factor of the physical models is 0.047 which according to the result (4.9), gives a frequency scale factor of 0.0866 if γ is taken to be 1.2. This is almost twice the physical scale factor of 0.047 and can quite significantly affect the spectra when small-scale model test data is extrapolated to full-scale conditions. To demonstrate this point, figure 9 plots the full-to-small-scale frequency ratio as a function of the physical dimension ratio, both for the conventional scaling and the Reynolds-number-dependent scaling (4.9). It is clear from the figure that the differences between the two can be quite significant for small-model tests. For practical applications, the figure indicates that for models larger than about 10% of the full-scale aircraft, the conventional frequency scaling may be sufficient, but for models less than about 10% of the full-scale geometry, frequencies have to be scaled according to the Reynolds-number-dependent scaling.

5. Effects of flap/slat settings

Clearly, the unsteady motions in the flow are strongly affected by the deployment of the flaps and slats. In the case of flaps, for example, their deployment results in pressure differences between the lower and the upper flap surface, which in turn drive the spanwise cross-flow. This cross-flow is believed to be highly unstable and to be the cause of the double-vortex formation in flap side edge regions. Thus, it can be expected that larger flap deployment angles would lead to more intense pressure fluctuations. This is indeed what we observed in our data. Some examples are shown in figures 10 and 11, which show the variations of surface pressure spectra with flap angles for $M = 0.275$, slats deployed at 20° and landing gears retracted. Figure 10 is for the sensor SP29, on the side surface of the outboard edge of the outboard flap, and figure 11 is for SP8, on the lower surface of the outboard edge of the inboard flap. The two sensors show quite different spectral characteristics, one dominated by the distinct spectral humps while the other shows a smooth fall-off with frequency, which will be discussed in more detail in the next section. However, the trends of the pressure amplitudes as a function of the flap angles are quite consistent for both. The higher the flap settings, the higher the surface-pressure amplitudes.

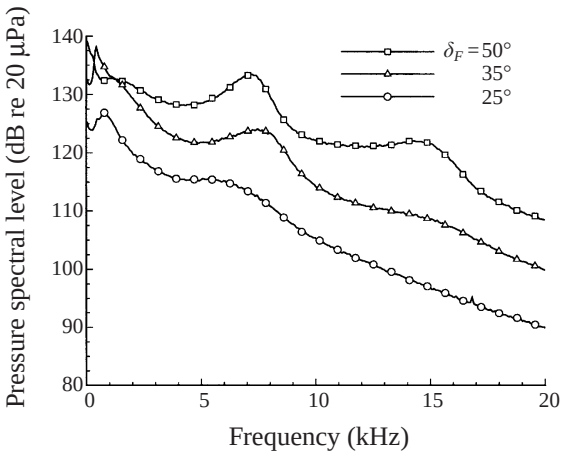

FIGURE 10. Surface pressure spectra for SP29, located on the side surface of the outboard edge of the outboard flap, at different flap settings with $M = 0.275$, slats deployed at 20° and landing gears retracted.

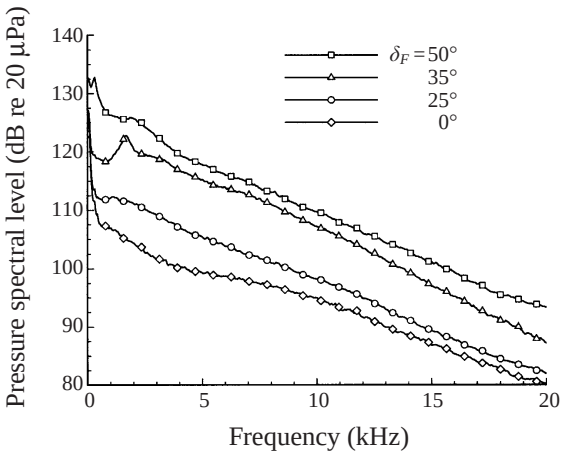

FIGURE 11. Surface pressure spectra for SP8, located on the lower surface of the outboard edge of the inboard flap, at different flap settings with $M = 0.275$, slats deployed at 20° and landing gears retracted.

Another example of this flap-angle dependence of the surface-pressure amplitude is shown in figure 12 for sensor SP29, the flap side surface sensor, at conditions with slats retracted as well as deployed at 20°. This figure also shows the effects of slat deployment on pressure on the flap surface. Since the sensors on the flaps are located far away from the slats, the pressure spectra are mainly controlled locally by the flap settings and are quite insensitive to changes in slat conditions. At large flap angles, 50°, for example, the local pressure fluctuations are dominated by local flows so that the slat deployment only causes a small change in the pressure amplitudes, as shown in figure 12 by the two curves indicated by the squares and triangles. At a flap angle of 35°, the local flap flow is more noticeably coupled to the slat conditions, though still weak. This shows up in the surface pressures on the flap. As can be seen in figure 12 from the two curves indicated by the deltas and circles, the deployment of a slat results in an amplitude increase of 2–3 dB in surface pressures on the flap.

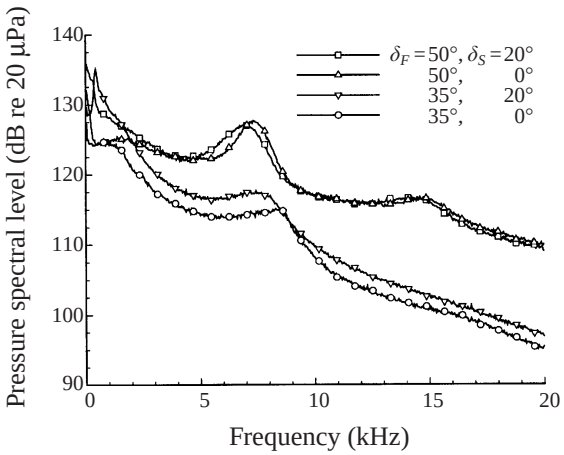

FIGURE 12. Comparison of surface pressure spectra for different flap and slat angles for $M = 0.275$ and landing gears retracted. The sensor is SP29 located on the side surface of the outboard edge of the outboard flap.

Figures 10 and 12 also show that the peak frequencies of the spectral humps vary with flap angles. Typically, when the flap angle varies from 50° to 35°, the peak frequency increases by about 1 kHz. Note that this frequency shift occurs between two cases that have the same mean flow Mach number and for the same model scale aircraft. These two parameters are conventionally used to determine the dominant frequency of the flow process. The frequency shift revealed in the two figures, however, indicates that this conventional approach may not be applicable here, for it would predict exactly the same frequency for all flap angles, contradicting what is shown in the data. This provides further support for the analysis given in the previous section on Strouhal-number scaling which uses flow-dependent characteristic lengths.

6. Surface pressures at other locations

The results in the above sections show that the surface pressures at the outboard edge of the outboard flap are dominated by the spectral humps associated with flow separation at the edge. We are intrigued to find that these spectral humps are largely absent at other locations on the flaps. This is already clear from figure 11 which shows the surface pressures at the outboard edge of the inboard flap. It is clear from this figure that the surface-pressure spectra do not contain the features associated with the spectral humps. To further demonstrate this, results for other sensors at this side edge location are shown in figure 13. Here, normalization is applied to both frequency and amplitude. The frequency normalization is carried out according to the Strouhal number definition (4.6) and the amplitude normalization is defined by

$$10 \log \frac{E(f) U_0}{q^2 \delta^*}, \tag{6.1}$$

where q is the free-stream flow dynamic head,

$$q = \tfrac{1}{2} \rho_0 U_0^2, \tag{6.2}$$

with ρ_0 and U_0, respectively, being the constant mean density and mean flow velocity. Clearly, for all the sensors, the spectral shapes are quite smooth with a gradual fall-

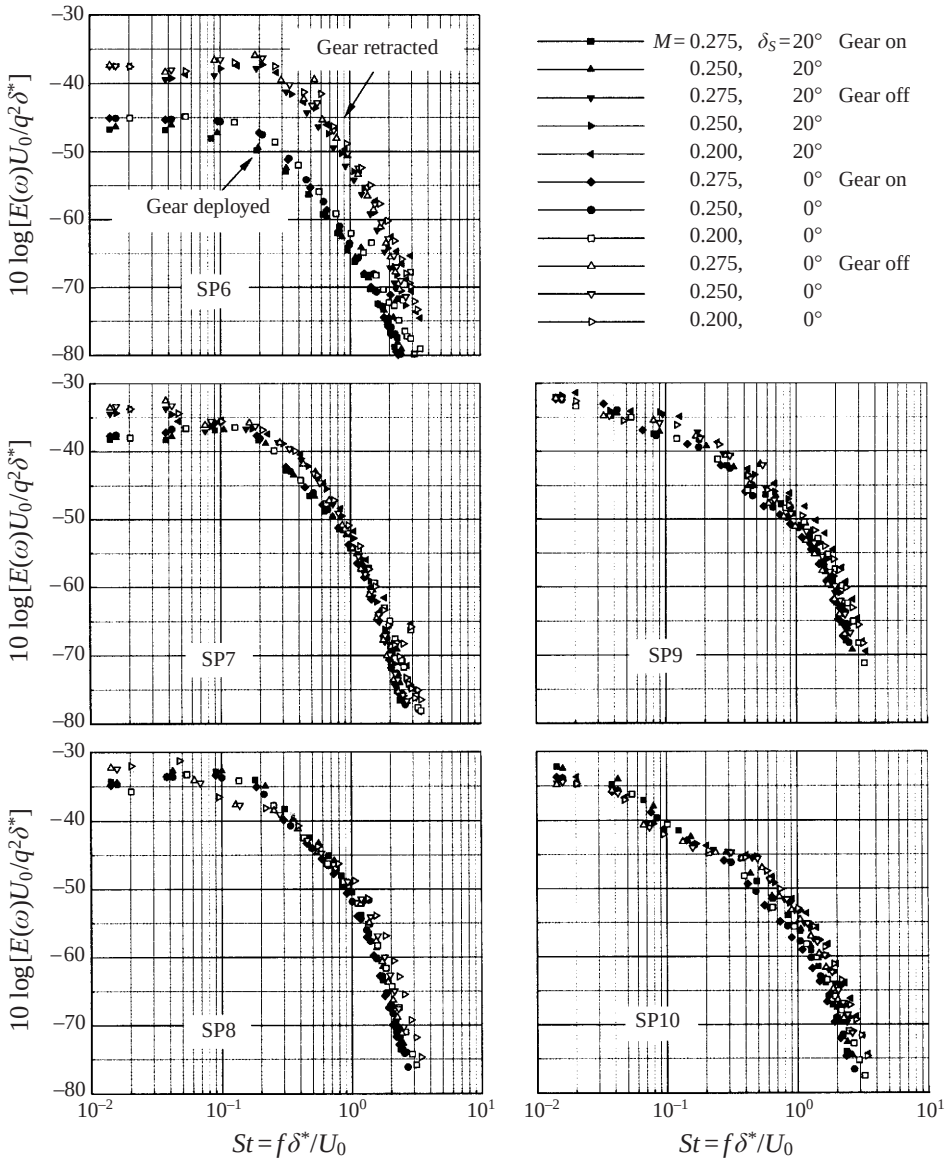

FIGURE 13. Normalized surface pressure spectra at different test conditions for sensors located at the outboard edge of the inboard flap with flaps deployed at 50°.

off with frequency and no distinct humps are present. In this non-dimensional form, the spectral shapes and amplitudes are both very similar to those for fully developed turbulent boundary-layer flows. For comparison, figure 14 plots the spectra for sensors at the mid-span location of the inboard flap, which is away from the flap side edges so that the flow there is dominantly trubulent boundary layer. Evidently, there is a close resemblance between these two figures. Both show a gradual fall-off with frequency without distinct spectral humps, both spectral shapes are bent downwards, indicating an inverse power law for frequency dependence and both have 5–10 dB higher spectral levels for upper surface sensors than those of the lower surface sensor.

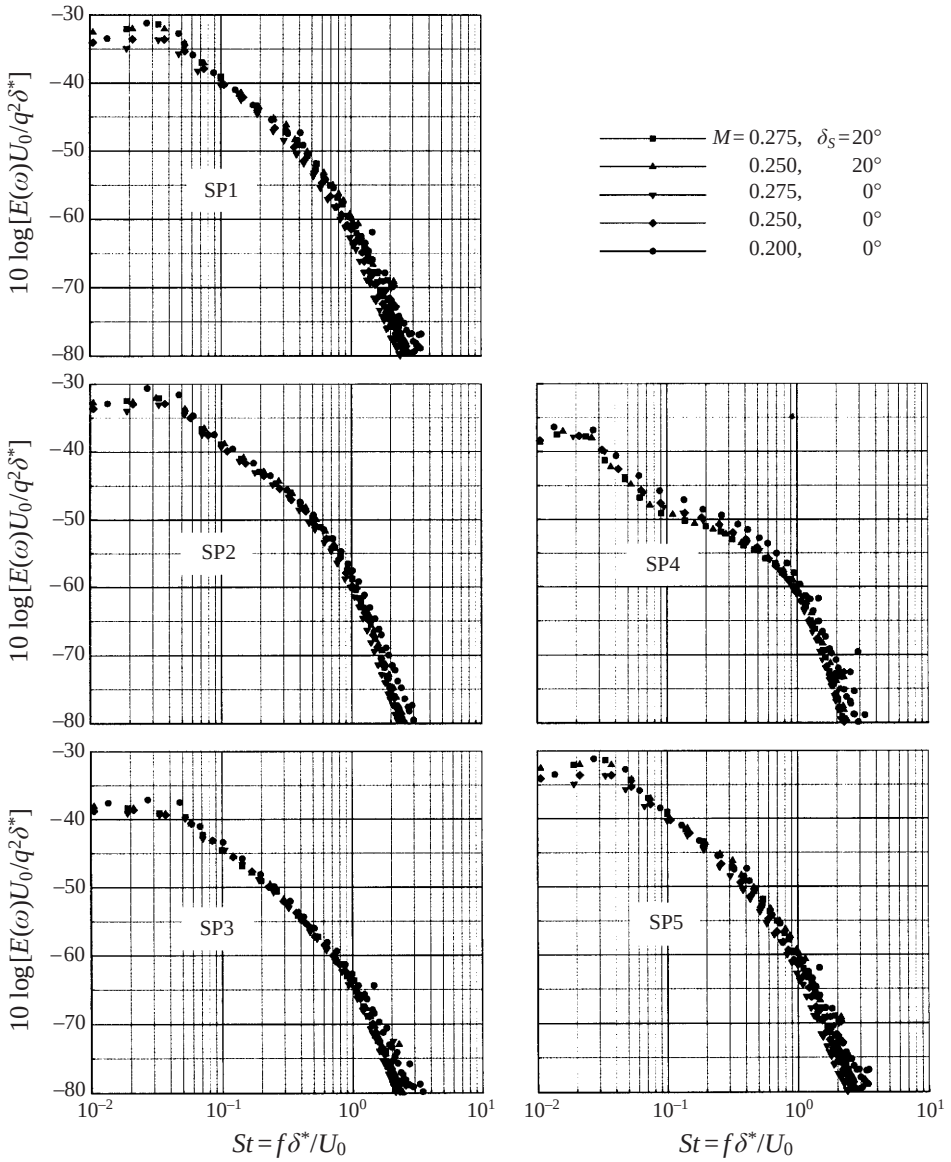

FIGURE 14. Normalized surface pressure spectra at different test conditions for sensors located at the mid-span of the inboard flap with flaps deployed at 50°.

All these are typical of fully developed turbulent flows and have been observed on isolated airfoils (e.g. Blake 1986; Brooks & Hodgson 1981).

It is not too difficult to understand the nature of the flow at the mid-span location (figure 14) because the flap geometry there makes the flow two-dimensional. Thus, the flow on the flap at mid-span locations is essentially fully developed turbulent boundary flow. It is, however, a surprise to find that the flow at the thrust gate, where there are two flap side edges, also behaves like fully developed turbulent flow with quite homogeneous features, as shown in figure 13. From the results given in the previous sections, it is known that side edge flow separation causes the formation of large-scale vortex structures. These structures are shown to dominate the flow at

the outboard edge of the outboard flap. It is then interesting to ask why the two other side edges do not see the dominance of the vortex structures. Without detailed flow measurements, it is difficult to draw any conclusion with confidence and further study is necessary. Here, we offer some possible explanations that are only partially supported by our limited data. The first possible reason is that the static pressure distribution has a smaller spanwise gradient at the thrust gate than that at the outboard edge of the outboard flap. This smaller static pressure gradient would make the flow separation, and thus, the vortex roll-up process, less intense at the edges near the thrust gate. The edges at the thrust gate are also in the wake of the nacelle and are affected by the main landing gears. The level of the turbulent incoming flow at this location can then be expected to be higher than that at the outboard edge of the outboard flap that is aerodynamically far away from both the nacelle and the landing gears. The joint effects of reduced flow separation and the higher turbulence levels would then bury the spectral humps due to flow separation in the broadband spectra owing to turbulent flow.

Another possible explanation for the reduced effects of flow separation at the edges near the thrust gate may be the edge raking effect. The edges at this location are not aligned with the mean flow direction; instead, they are raked into the flow. In simple terms, an edge raked into the flow behaves more like a leading edge with the incoming flow impinging on it, whereas an edge raked away from the flow is more like a trailing edge with flow leaving it. Thus, the flow at the outboard edge of the outboard flap, which is raked away from the flow, is very favorable for flow separation, in the form of vortex shedding, similar to trailing edges. At the thrust gate, the edges are raked into the flow, making the edge/flow interaction similar to that of leading edges. In this case, conditions for flow separation are less favorable. This reduces the effects of flow separation in the surface pressures. This effect of raking has actually been observed in experiments using simple model flaps (Storms *et al.* 1998) where it is observed that raking into the flow reduces the noise associated with the flap side edge, probably by reducing the flow separation as analysed above.

7. Far-field/near-field correlation

The coherence of the three surface sensors in the aft half-chord region at the outboard edge of the outboard flap with far-field noise is shown in figure 15 for the test conditions of $M = 0.275$, slats deployed at 20° and landing gear retracted. The coherence is quite low except in the band of about 6–9 kHz, that is the band of the spectral humps seen in the surface pressures in the previous section. Again, this figure is representative of other test conditions. This shows that the spectral humps in the surface pressures do have acoustic radiation. The correlations of the same three sensors with the far field is shown in figure 16, which are computed from the complex coherence functions in the frequency band of 6–9 kHz. Again, it is shown here that the surface pressure fluctuations in this frequency band are indeed correlated to the far-field noise. The correlations in this figure have a time delay of about 3.5 ms, which is the same as the time needed for a sound wave to travel from the outboard edge of the outboard flap to the free field microphone that is located about 4.25 feet below the wing. The wave-package-like shape of the correlation coefficients also reflects the nature of the noise source. The source is neither narrow nor broadbanded; it covers a broad spectral hump, leading to the Gaussian-shaped correlation coefficient with rapid oscillations within it.

When the correlation analysis is applied to other locations on the wing, we find that

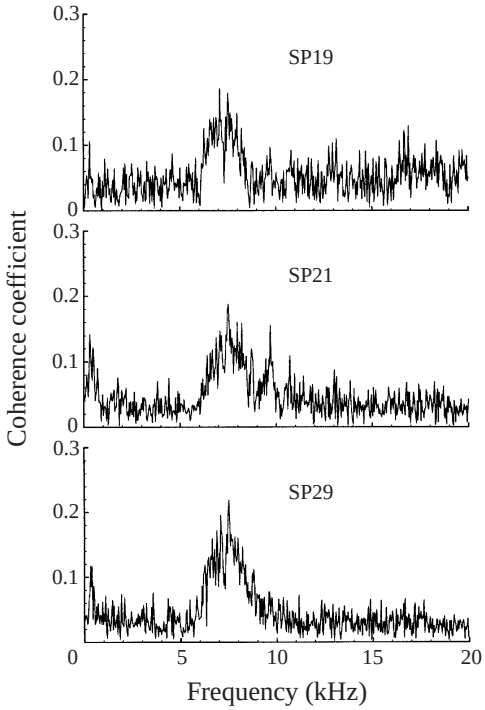

FIGURE 15. Coherence between far-field sound pressure and surface pressures in the aft half-chord region at the outboard edge of the outboard flap for $M = 0.275$, flaps and slats deployed, respectively, at 50° and 20° and landing gears retracted.

the outboard edge of the outboard flap is the location that has the best correlation with far-field noise. This is demonstrated in figure 17, which plots correlation between far-field noise and five surface sensors located on the lower surface of the wing at different spanwise locations, for the same test conditions as in figure 16. The correlation is for the frequency band of 6–9 kHz. The plots in this figure clearly show that the dominant source for the noise in this frequency band is in the region close to the outboard edge of the outboard flap. In another test using the same aircraft model, we find that measurements by using a phased microphone array show strong sources at the outboard edges of the flaps but not at the inboard edge (Guo *et al.* 1998), which is consistent with what is revealed in figure 16.

In analysing the far-field/near-field correlation, we find that, though definite coherence/correlation can be seen in certain frequency bands, the values of the coherence and correlation coefficients are quite low, typically of the order of or below 0.2 (figures 15–17, for example). This kind of coherence level is low in comparison with those among near-field quantities themselves, such as those shown in previous sections between surface pressure sensors, but is consistent with other experimental studies on airfoils and wings in the same or similar facilities. For example, Miller, Meecham & Ahtye (1982) conducted a semi-span wing test in the same NASA Ames 40×80 feet wind tunnel and they reported correlation levels of the order of 0.1. The correlations in that study are defined as that between surface pressure and the time derivative of the far-field pressure, which is slightly different from those used here in our analysis which are pressure/pressure correlation. When our results are computed following the same definition for the correlation coefficients as in Miller *et al.* (1982), the max-

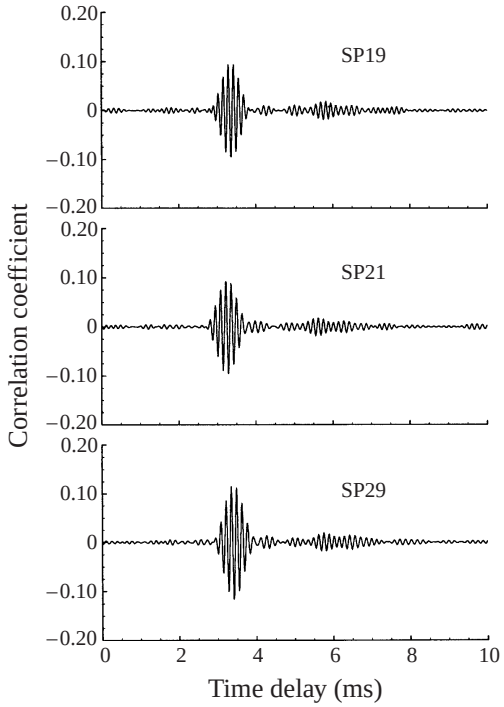

FIGURE 16. Correlation between far-field sound pressure and surface pressures in the aft half-chord region at the outboard edge of the outboard flap for $M = 0.275$, flaps and slats deployed, respectively, at 50° and 20° and landing gears retracted.

imum value of the correlation for our DC10 model is found to be about 0.1, of the same order as those reported in Miller *et al.* (1982). Another experiment involving airfoil tip flow is that by McInerny *et al.* (1986), performed with an isolated airfoil in the NASA Ames 7×10 feet wind tunnel, which is not acoustically treated either. The far-field/near-field correlation in that study has even smaller values, about 0.03 maximum. This is probably because the NASA Ames 7×10 feet tunnel is even noisier than the partially treated 40×80 feet wind tunnel, and thus further corrupting the far-field/near-field correlation. The above comparison between different tests shows the consistency of our results with others and also implies that airframe noise tests in untreated wind tunnels may have to face the low levels of far-field/near-field correlation. This is probably because airframe noise has multiple incoherent sources and each source is distributed in space. The sources at different locations may be acoustically decoupled in that their contributions to the far-field noise are additive, but these sources may be aerodynamically coupled to each other in that changes in one source may affect the strength of others, and thus, affecting the sound/surface pressure correlation.

8. Effects of flap side edge fences

As a means of reducing flap-related noise, flap side edge fences are tested. As reported in Guo *et al.* (1998) and elsewhere (Ross *et al.* 1995; Storms *et al.* 1996), side edge fences can reduce flap related noise by a few dB, but the exact mechanisms by which the noise is reduced have not been fully understood. The general concept

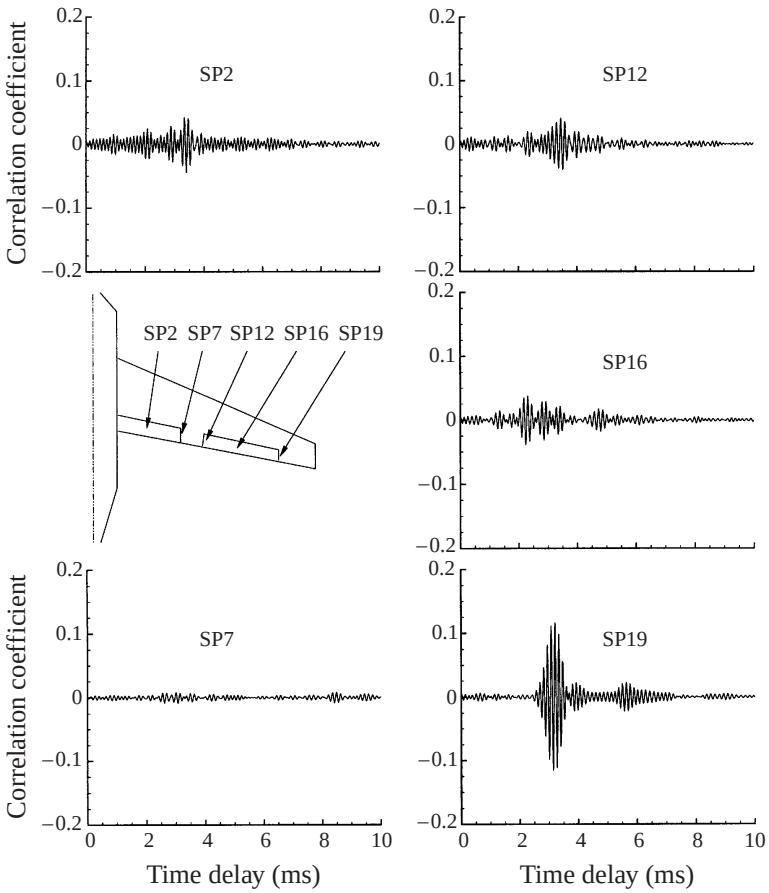

FIGURE 17. Correlation between far-field sound pressure and surface pressures at different spanwise locations on the lower surface of the high-lift system for $M = 0.275$, flaps and slats deployed, respectively, at 50° and 20° and landing gears retracted.

of using fences is to modify the local geometry so that the unsteady flows, and hence, the noise sources, are correpondingly modified. The reduction in noise levels in the far field indicates that the noise sources are indeed affected by the fences. In this section, we offer a possible mechanism, based on our surface-pressure data, to explain the effects of flap side edge fences.

Our analysis is based on the concept that flap-related noise is generated by the double-vortex structure in the flap side edge region, and the evolution of this vortex structure is strongly affected by the thickness of the flap. The flap thickness determines the helical roll-up path along which the vortex can evolve. The evolution of the vortex gives the characteristic lengthscale of the flow, which, together with the typical cross-flow velocity, sets the timescale of unsteady motions. When a side edge fence is applied, it effectively increases the flap thickness, and thus, increases the evolution path. This, in turn, leads to a longer timescale. In frequency domain, this manifests itself as a decrease in peak frequency. This is, in fact, what we observed in our surface-pressure data. To demonstrate this, figure 18 plots the pressure spectra of SP19 and SP21, respectively, on the lower and upper surface of the flap at the outboard edge of the outboard flap, for the cases with and without the fences. The test conditions

in this figure are $M = 0.275$, flaps deployed at 50° and both slats and landing gears retracted. The most noticeable feature in this figure is that the spectral humps are present for all cases, with or without the fences, and that the peaks of the spectral humps shift to lower frequencies as the height of the fences increases. This confirms our analysis that the effects of the flap side edge fences are essentially to increase the evolution time of the vortex structure, leading to lower frequencies for the unsteady motions. As can be expected, the lower frequencies also manifest themselves in the coherence of the near-field quantities, which is illustrated in figure 19 through the coherence between SP19 and SP21. Without the fence, high coherence of about 0.8 is seen at about 7.5 kHz. When the fences are applied, and as the height of the fence increases, the peak frequency of the coherence gradually decreases. Another noticeable feature shown in figures 18 and 19 is that the decrease in peak frequency is not proportional to the increase of the flap fence height. This provides further support to our analysis in previous sections on the characteristic lengthscale of the flow process, namely, the characteristic length should be flow dependent, instead of simply the model dimension. If the effective flap thickness (flap plus fence) were used as the reference lengthscale to estimate the peak frequency, doubling the thickness (the case with fence 1) would lower the frequency by half from 7.5 kHz to approximately 3.75 kHz. However, our data show that the peak frequency for this case is about 2.5 kHz, indicating a significant error in the estimate if the flat side surface dimension is used as the reference lengthscale.

The changes in the near-field flow owing to the side edge fences also effect the sound/surface pressure coherence. This is shown in figure 20 by the coherence between far-field noise and the surface pressure at SP19, the sensor on the lower surface near the outboard edge of the outboard flap. Apart from the use of different fences, all four cases in this figure have identical flow conditions and identical wing configurations; they all have $M = 0.275$, flaps deployed at 50° and both slats and landing gears retracted. The bottom diagram is for the case without a fence, which shows high coherence at 7.5 kHz. The next diagram is for the smallest fence, fence 3 that has a height of half flap thickness. For this fence, the peak frequency of the sound/surface pressure coherence is shifted from 7.5 kHz for the case without fences downward to about 3 kHz, and the width of the frequency domain is also reduced. These trends continue as the fence height increases from half flap thickness to one flap thickness and then to twice the flap thickness, shown in the top diagram. For the largest fence, the side edge fences essentially suppress the coherence.

The downward shift of the dominant frequency in the spectra of the flow fluctuations shown in our data provides a possible explanation for the noise reduction due to flap side edge fences observed in many tests (Ross *et al.* 1995; Storms *et al.* 1996; Guo *et al.* 1998). This is because far-field noise spectra are in general determined by the spectra of near-field fluctuations so that a downward frequency shift in the near-field flow also causes a similar downward frequency shift in the far-field noise. Even without any reduction in source strength, this downward shift in frequency may appear as a noise reduction. This is because airframe noise typically has a spectrum with a negative slope in almost the entire mid- to high-frequency domain, which is also the most sensitive domain for aircraft noise certification. Thus, for any fixed frequency bands, a downward shift of the spectrum replaces the noise levels in these bands with the lower levels at higher frequencies. In this way, a reduction in noise level is achieved for fixed frequency bands even if the total radiated acoustic energy remains unchanged. The mechanism of the noise reduction is then to shift some spectral energy out of the frequency bands that are of interest to noise certification.

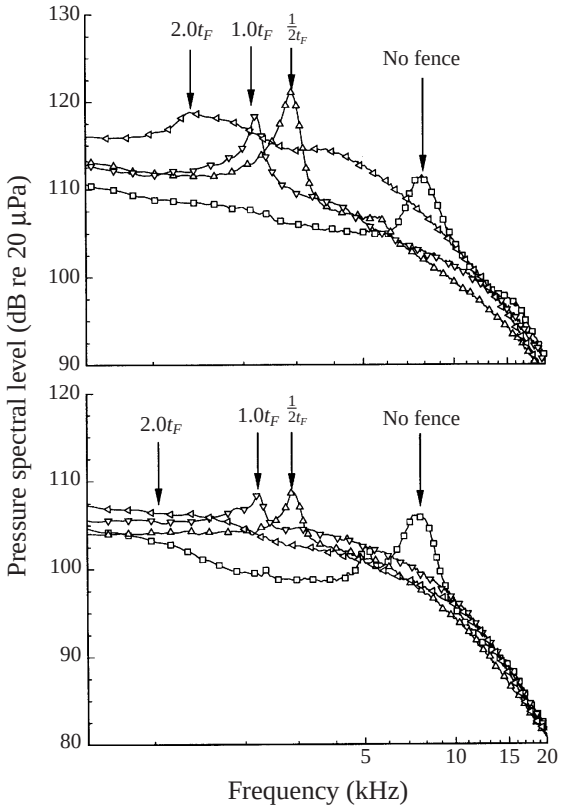

FIGURE 18. Surface pressure spectra for different flap side edge fences. The upper diagram is for SP21 and the lower diagram for SP19, both located at the outboard edge of the outboard flap but, respectively, on the upper and lower surface. Note the downward shift of the hump frequency as the fence height increases.

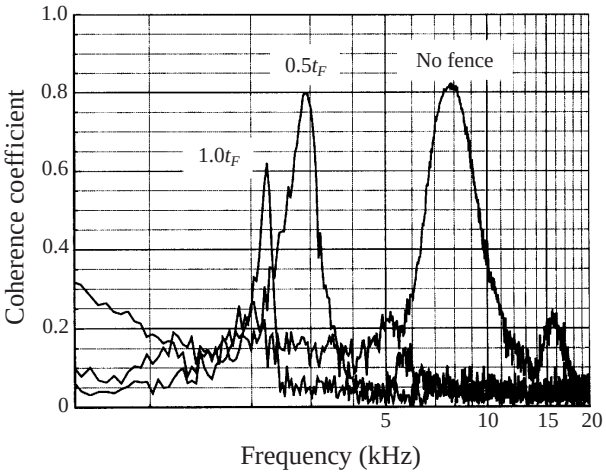

FIGURE 19. Effects of different flap side edge fences on the cross-coherence between SP21 and SP19, both located at the outboard edge of the outboard flap with the former on the upper surface and the latter on the lower surface.

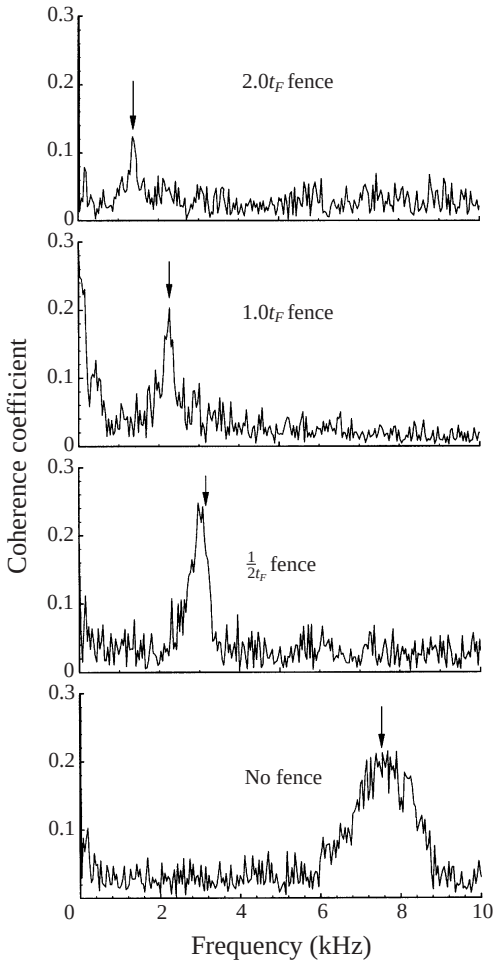

FIGURE 20. Correlation between far-field sound and unsteady surface pressures at SP19 for different flap side edge fences, showing the downward shift of the peak coherence frequency with fence height.

Our limited database does not enable us to show conclusively whether there is a weakening in source strength due to the fences, which may also contribute to the observed reduction in far-field noise. Our data, however, does reveal the downward shift in characteristic frequencies of the flow features. Hence, at least some part of the noise reduction due to flap side edge fences may come from the shift of the acoustic energy out of the frequency bands that are important to aircraft noise certification.

9. Conclusions

In this paper, we have analysed surface pressure fluctuations on aircraft flaps and their correlation with far-field noise. It has been shown that the surface pressure fluctuations, in general, increase with flow Mach number, flat and slat angles. The vortex structure associated with flow separation in the flap side edge flow has been shown to manifest itself in the surface pressure spectra in the form of distinct spectral humps. This is most clearly seen at the outboard edge of the outboard

flap where the incoming flow has low turbulence level and the edge is raked away from the flow direction, providing a favorable condition for flow separation. For side edges embedded in turbulence of high levels and/or raked into the flow, the surface pressures show characteristics of fully developed turbulent flows. At the edge, where local flow separation dominates, the spectral humps are highly coherent and are well correlated to far-field noise. The surface pressures have been scaled on Strouhal number with flow-dependent lengthscales. This Strouhal number scaling leads to a frequency extrapolation from small-scale test data to full-scale that is different from the conventional method and is shown to be important for small models less than about 10% of the full-scale dimension. Analysis of data for the cases with flap side edge fences has shown that the most noticeable effects of the fences is the downward shift of the dominant frequency in the surface pressure spectra, in the surface pressure cross-coherence and in the far-field/near-field correlation. Based on this, a possible explanation for the noise reduction mechanism due to flap side edge fences has been proposed, which attributes the noise reduction to the shift of spectral energy out of the frequency bands that are important to noise certification.

The work presented in this paper is sponsored by the NASA Advanced Subsonic Technology Program (under the Noise Reduction Element). The authors would like to thank the group of people at NASA Ames Research Center, C. J. Ross, P. T. Soderman, D. Ashby, B. L. Storms, J. A. Hayes, M. Watts and M. Mosher, to name just a few, who made the test a success. The authors would also like to thank the task monitor, Dr W. C. Horne of NASA Ames Research Center, for his support and encouragement.

REFERENCES

Ahtye, W. F., Miller, W. R. & Meecham, W. C. 1979 Wing and flap noise measured by near and far field cross-correlation technique. *AIAA Paper* 79-0667.

Allen, C. S. & Soderman, P. T. 1997 Scaling and extrapolating small-scale in-flow wind tunnel jet noise to full scale fly-over jet noise. *AIAA Paper* 97-1602.

Blake, W. K. 1986 *Mechanics of Flow-Induced Sound and Vibration*. Academic.

Brooks, T. F. & Hodgson, T. H. 1981 Trailing edge noise prediction from measured surface pressures. *J. Sound Vib.* **78**, 69–117.

Curle, N. 1955 The influence of solid boundaries upon aerodynamic sound. *Proc. R. Soc. Lond.* A **231**, 505–514.

Ffowcs Williams, J. E. & Hawkings, D. L. 1969 Sound generation by turbulence and surfaces in arbitrary motion. *Phil. Trans. R. Soc. Lond.* A **264**, 321.

Guo, Y. P. 1999 Prediction of flap edge noise. *AIAA Paper* 99-1804.

Guo, Y. P., Hardy, B. A., Bent, P. H., Yamamoto, K. J. & Joshi, M. C. 1998 Noise characteristics of DC-10 aircraft high lift systems. *NASA Contract Report*, CRAD-9310-TR-4893.

Hayes, J. A., Horne, W. C., Soderman, P. T. & Bent, P. H. 1997 Airframe noise characteristics of a 4.7% scale DC-10 model. *AIAA Paper* 97-1594.

Horne, W. C., Hayes, J., Ross, J. C. & Storms, B. L. 1997 Measurements of unsteady surface pressure fluctuations on the surface of an unswept, multi-element airfoil. *AIAA Paper* 97-1645.

Howe, M. S. 1978 A review of the theory of trailing edge noise. *J. Sound Vib.* **61**, 437–465.

Khorrami, M. R., Singer, B. A. & Radeztsky, R. H. 1998 Reynolds averaged Navier–Stokes computations of a flap side-edge flow field. *AIAA Paper* 98-0768.

McInerny, S. A., Meecham, W. C. & Soderman, P. T. 1986 An experimental investigation of wing tip turbulence with applications to aerosound. *AIAA Paper* 86-1918.

McInerny, S. A., Meecham, W. C. & Soderman, P. T. 1990 Pressure fluctuations in the tip region of a blunt-tipped airfoil. *AIAA J.* **28**, 6–13.

Mathias, D. L., Roth, K. R., Ross, J. C., Rogers, S. E. & Cummings, R. M. 1995 Navier–Stokes analysis of the flow about a flap edge. *AIAA Paper* 95-0185.

Meadows, K. R., Brooks, T. F., Humphery, W. M., Hunter, W. H. & Gerhold, C. H. 1997 Aeroacoustic measurements of a wing flap configuration. *AIAA Paper* 97-1595.

Miller, W. R., Meecham, W. C. & Ahtye, W. F. 1982 Large scale model measurements of airframe noise using cross-correlation technique. *J. Acoust. Soc. Am.* **71**, 591–599.

Radeztsky, R. H., Singer, B. A. & Khorrami, M. R. 1998 Detailed measurements of a flap side-edge flow field. *AIAA Paper* 98-0700.

Ross, J. C., Storms, B. L. & Kumagai, H. 1995 Aircraft flyover noise reduction using lower-surface flap-tip fences. *NASA CDTM*-21006.

Storms, B. L., Takahashi, T. T., Horne, W. C., Ross, J. C., Dougherty, R. P. & Underbrink, J. R. 1996 Flap-tip treatments for the reduction of lift-generated noise. *NASA CDTM*-21006.

Storms, B. L., Ross, J. C., Horne, W. C., Hayes, J. A., Doughterty, R. P., Underbrink, J. R., Scharpf, D. F. & Moriarty, P. J. 1998 An aeroacoustic study of an unswept wing with a three-dimensional high lift system. *NASA/TM*-1998-112222.